AGU PUBLICATIONS

JGR

Journal of Geophysical Research: Atmospheres

RESEARCH ARTICLE
10.1002/2016JD025138

Key Points:
- Humid watersheds show increased uncertainty in projecting the changes in hydrologic attributes
- CIE-GCM primarily accounts for unexplained changes in mean and variability of seasonal streamflow
- CIE-TD and CIE-SIM account for inability to explain the changes in seasonal extremes in streamflow

Supporting Information:
- Supporting Information S1

Correspondence to:
S. B. Seo,
sseo@ncsu.edu

Citation:
Seo, S. B., T. Sinha, G. Mahinthakumar, A. Sankarasubramanian, and M. Kumar (2016), Identification of dominant source of errors in developing streamflow and groundwater projections under near-term climate change, *J. Geophys. Res. Atmos.*, *121*, doi:10.1002/2016JD025138.

Received 27 APR 2016
Accepted 12 JUN 2016
Accepted article online 17 JUN 2016

Identification of dominant source of errors in developing streamflow and groundwater projections under near-term climate change

S. B. Seo[1], T. Sinha[2], G. Mahinthakumar[1], A. Sankarasubramanian[1], and M. Kumar[3]

[1]Department of Civil, Construction, and Environmental Engineering, North Carolina State University, Raleigh, North Carolina, USA, [2]Department of Environmental Engineering, Texas A&M University–Kingsville, Kingsville, Texas, USA, [3]Nicholas School of Environment, Duke University, Durham, North Carolina, USA

Abstract Uncertainties in projecting the changes in hydroclimatic variables (i.e., temperature and precipitation) under climate change partly arises from the inability of global circulation models (GCMs) in explaining the observed changes in hydrologic variables. Apart from the unexplained changes by GCMs, the process of customizing GCM projections to watershed scale through a model chain—spatial downscaling, temporal disaggregation, and hydrologic model—also introduces errors, thereby limiting the ability to explain the observed changes in hydrologic variability. Toward this, we first propose metrics for quantifying the errors arising from different steps in the model chain in explaining the observed changes in hydrologic variables (streamflow and groundwater). The proposed metrics are then evaluated using a detailed retrospective analyses in projecting the changes in streamflow and groundwater attributes in four target basins that span across a diverse hydroclimatic regimes over the U.S. Sunbelt. Our analyses focused on quantifying the dominant sources of errors in projecting the changes in eight hydrologic variables—mean and variability of seasonal streamflow, mean and variability of 3 day peak seasonal streamflow, mean and variability of 7 day low seasonal streamflow, and mean and standard deviation of groundwater depth—over four target basins using an Penn state Integrated Hydrologic Model (PIHM) between the period 1956–1980 and 1981–2005. Retrospective analyses show that small/humid (large/arid) basins show increased (reduced) uncertainty in projecting the changes in hydrologic attributes. Further, changes in error due to GCMs primarily account for the unexplained changes in mean and variability of seasonal streamflow. On the other hand, the changes in error due to temporal disaggregation and hydrologic model account for the inability to explain the observed changes in mean and variability of seasonal extremes. Thus, the proposed metrics provide insights on how the error in explaining the observed changes being propagated through the model under different hydroclimatic regimes.

1. Introduction

Potential impacts of climate change on water resources management have received considerable attention in recent decades due to continually increasing global temperature. Consequently, many studies have focused on assessment of climate change impacts on hydrologic variables [*Cherkauer and Sinha*, 2010; *Vano et al.*, 2010; *Cheng et al.*, 2012; *Harding et al.*, 2012; *Ficklin et al.*, 2013; *Koutroulis et al.*, 2013; *Yang et al.*, 2014]. Mostly, precipitation and temperature projections that are simulated by global circulation models (GCMs) forced with hydrologic models to quantify the potential changes in hydrologic variables as well as the impacts on water resources [*Cherkauer and Sinha*, 2010; *Cheng et al.*, 2012; *Harding et al.*, 2012; *Ficklin et al.*, 2013; *Yang et al.*, 2014]. Nevertheless, it is well known that there is considerable uncertainty in developing hydroclimatic projections using GCM outputs [*Maurer and Duffy*, 2005]. Hence, studies have focused on reducing and quantifying the uncertainty in hydroclimatic projections [*Maurer and Duffy*, 2005; *Hawkins and Sutton*, 2009; *Woldemeskel et al.*, 2012; *Katz et al.*, 2013]. Apart from uncertainty arising from GCMs, efforts have also focused on uncertainties arising from the model chain—the suite of physical and statistical models by which large-scale climate change information is translated to local/regional impacts—in developing hydroclimatic projections [*Najafi et al.*, 2011; *Yip et al.*, 2011; *Bosshard et al.*, 2013; *Thompson et al.*, 2013; *Woldemeskel et al.*, 2014]. For instance, *Wilby and Harris* [2006] have considered uncertainties in low-flow scenarios for Thames River basin due to emission scenarios, GCMs, statistical downscaling, and hydrologic model structure. These studies, however, have primarily employed analysis of variance (ANOVA) techniques on quantifying the uncertainties contributed

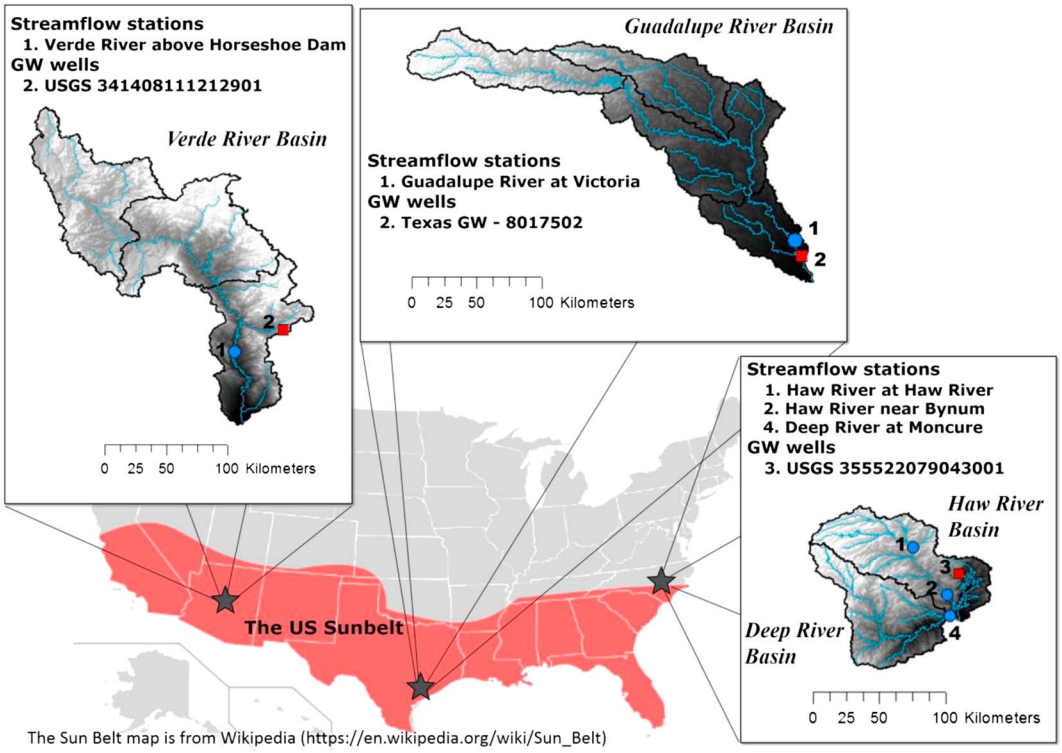

Figure 1. Selected four target basins across the U.S. Sunbelt.

by the model chain on the-end-of-the-century projections, which of course does not consider the uncertainty in estimating observed estimates. Besides, *Woldemeskel et al.* [2014] addressed how GCM uncertainties affect hydrologic impact assessment models by quantifying and accounting for GCM uncertainties in drought assessment model. On the contrary, this study focuses on decomposing the sources of errors in developing hydroclimatic projections using GCM forcings of CMIP5 (Coupled Model Intercomparison Project Phase 5) through a detailed retrospective analysis by comparing with the observed hydroclimatic data.

CMIP5 projections provide multiple GCM simulations under different climate change scenarios until the end of the century (~2100) [*Taylor et al*., 2012a]. CMIP5 also includes decadal hindcasts that were developed by initializing GCMs with SSTs (sea surface temperatures) over various time periods to develop 10 year and 30 year hindcasts [*Taylor et al*., 2012a]. *Hawkins and Sutton* [2009] showed that emission scenarios represent most uncertainty when it comes to the end-of-the-century projections, but for near-term (10–30 years) climate change projections, uncertainty due to climate models is expected to be significant. Since most water resources planning typically focuses on 10–30 year time scales, one could utilize near-term hydroclimatic projections for supporting basin-wide planning and water allocation decisions [*Singh et al*., 2015]. Another advantage in focusing over 10–30 year time scales stems from the reduced uncertainty induced by emission scenarios in near-term climate change scenarios [*Hawkins and Sutton*, 2009]. Hence, we focused on the relative contribution of errors from multiple steps in the model chain in developing near-term hydroclimatic projections by comparing with the eight observed changes in hydrologic variables.

The main intent of this study is to decompose different sources of errors that arise in the model chain—spatially downscaled GCM forcings, temporal disaggregation, and hydrologic model—in estimating the changes in hydrologic variables from near-term climate change projections. For this purpose, we performed a retrospective analysis over four target basins from the U.S. Sunbelt (Figure 1) and compare the observed changes in streamflow and groundwater depth from the target period (1956–1980) to the control period (1981–2005) with the estimated changes using Penn State Integrated Hydrologic Model (PIHM) forced with CMIP5 projections. Errors in estimating the changes in streamflow and groundwater depth are then attributed to various steps in the model chain using a unique experimental design. Emission scenarios were not considered since GCM historic simulations were used for decomposing different sources of errors in estimating the observed changes

in hydrologic attributes. Given that our retrospective analyses compares the estimated changes from GCM projections with the observed changes in various hydrologic attributes, it provides a baseline for addressing the following science questions: (1) how can we attribute the errors in estimating the changes in seasonal streamflow and groundwater projections to different sources—spatially downscaled GCM forcings, temporal disaggregation, and hydrologic model—in the model chain? (2) what are the metrics that can systematically decompose and identify the sources of errors in projecting the changes in hydrologic attributes arising from the model chain in using climate change information? (3) what is the dominant source of error in the model chain and how does that dominant source vary in estimating the changes in seasonal hydrologic attributes as opposed to estimating the changes in seasonal extremes? and (4) how does each source of error vary under different seasons (e.g., winter versus summer) and four watersheds under different hydroclimatic regimes (e.g., arid versus humid)?

The manuscript is arranged as follows: section 2 details the selected pilot basins, models, and data used in this study. Section 3 describes the experimental design of the proposed error decomposition from the model chain along with associated performance metrics. Following that, results and analyses on error decomposition from the retrospective analyses are presented in section 4. Finally, the findings from the study are summarized followed by a discussion.

2. Hydroclimatic Data and Integrated Surface Water and Groundwater Model Setting

2.1. Study Area

We considered four different watersheds from the U.S. Sunbelt having both surface water and groundwater data over a long period of time. We selected four target basins—Haw River in NC, Deep River in NC, Guadalupe River in TX, and Verde River in AZ—which are located in varied hydroclimatic settings ranging from humid east to arid west (Figure 1). The Haw and Deep River basins together form the upper Cape Fear River basin, NC, that is located in the eastern part of the U.S. Sunbelt. The headwaters of the Haw River run 177 km into the Jordan Lake reservoir and the drainage area of the basin is 3959 km^2. The Deep River is approximately 201 km long and flows into the Haw River just downstream of Jordan Lake that supplies water for the Triangle area in NC [*Li et al*., 2014; *Singh et al*., 2015]. Both the Haw and the Deep River basins receive mean annual precipitation of 1137 and 1153 mm, respectively. The Guadalupe River, a semiarid basin located in Texas, flows to the San Antonio Bay which drains into the Gulf of Mexico. The drainage area of the Guadalupe River basin is 11,860 km^2, and it receives a mean annual precipitation of 858 mm. Recharge from the Guadalupe River partly goes into the Edwards aquifer, which supplies water to the city of San Antonio [*Clark et al*., 2014]. Observed streamflow in the Guadalupe River does not exhibit seasonality with monthly flows being uniformly distributed over the year. The Verde River, an arid basin, covers approximately 14,115 km^2 of north-central Arizona, which receives mean annual precipitation of 474 mm. The Verde River supplies water to the Phoenix metro area and is a part of the lower Colorado River basin.

2.2. Penn State Integrated Hydrologic Model (PIHM)

Many hydrologic models have been applied for quantitative projections of streamflow in studies that addressed climate change impact. However, most studies considered only the surface water or groundwater for quantifying the change projections [e.g., *Christensen et al*., 2004; *Fowler et al*., 2007; *Vicuna et al*., 2007; *Minville et al*., 2010; *Zhu and Ringler*, 2012; *Taylor et al*., 2012b; *Aich et al*., 2013; *Kløve et al*., 2014]. Even though several studies have developed a model of streamflow and groundwater coupling for simulating surface water, groundwater, and stream-aquifer interactions on a continuous basis (e.g., SWAT-MODFLOW model by *Kim et al*. [2008]), such couplings are primarily one way along the topographic gradient and do not capture water transfer in both directions. An integrated surface water and groundwater model, PIHM (Penn State Integrated Hydrologic Model), was used for ensuing analyses. PIHM is a fully coupled multiprocess model in which surface water, groundwater, and land surface components are fully coupled using a semidiscrete finite volume approach [*Qu and Duffy*, 2007]. Readers are referred to *Kumar* [2009] for more details about the individual process equations. The model has been successfully applied at multiple scales and in diverse hydroclimatological settings in both North America and Europe [*Shi et al*., 2013; *Wang et al*., 2013; *Yu et al*., 2014; *Chen et al*., 2015]. Since PIHM is a fully distributed model, it requires intensive data development and topology definitions. All physiographic and hydroclimatic data and other topological relations needed to perform model simulations are automatically mapped using PIHMgis [*Bhatt et al*., 2014].

Table 1. Stream Gauges and Groundwater Wells Selected for the Error Decomposition Analyses Over the Four Target Basins

Watershed	Station Name/Number	Longitude	Latitude	Data Availability	Aquifer Type/Depth
		Streamflow			
Haw River	At Haw River	79.366111	36.087222	1929–present	
Deep River	At Moncure	79.116111	35.626944	1931–present	
Guadalupe River	At Victoria	97.012778	28.792778	1934–present	
Verde River	Above Horseshoe dam	111.715556	34.073056	1946–present	
		Groundwater			
Haw River	USGS 355522079043001	79.058056	35.908611	1949–present	unconfined/ 48.0 ft
Guadalupe River	TWDB[a] 8017502	96.948888	28.684166	1993–present	unconfined/ 1026 ft
Verde River	USGS 341408111212901	111.358056	34.235556	1976–1988	unconfined/ 44.5 ft

[a]TWDB: Texas Water Development Board.

2.3. Data

2.3.1. Observed Precipitation, Temperature, Streamflow, and Groundwater Data Sets

Gridded observed precipitation and temperature data were downloaded from the following data link (http://www.engr.scu.edu/~emaurer/gridded_obs/index_gridded_obs.html) which is originally from Hydro | Computational Hydrology group in University of Washington (http://uw-hydro.github.io/). Monthly or daily gridded observations at 1/8° spatial resolution, roughly 12 km × 12 km, are now available up to 2010 and details regarding these data are described in *Maurer et al*. [2002]. Streamflow and groundwater data for four target basins are obtained from USGS (United States Geological Survey) Water Data webpage (http://waterdata.usgs.gov/nwis/) and Water Data for Texas webpage (http://www.waterdatafortexas.org/groundwater/). All streamflow gauges are HCDN (Hydroclimatic Data Network) stations which are located

Table 2. Seasonal Statistics of the six Observed Hydrologic Variables of Streamflow for the Target Basins During the Control Period[a]

		DJF	MAN	JJA	SON
		Seasonal Mean Streamflow			
Seasonal mean streamflow	Haw	23.1	21.0	9.8	10.9
	Deep	65.8	60.9	24.2	20.7
	Guadalupe	61.2	65.1	51.6	68.8
	Verde	27.2	25.7	5.7	10.1
		Seasonal Mean 3 Day Peak Flow			
Seasonal mean 3-day peak flow	Haw	125.4	103.6	67.1	82.1
	Deep	374.7	339.2	203.6	174.8
	Guadalupe	279.5	315.0	285.6	318.6
	Verde	261.0	160.4	19.4	89.7
		Seasonal Mean 7 Day Low Flow			
Seasonal mean 7-day low flow	Haw	6.7	5.9	2.7	2.7
	Deep	11.7	12.4	3.4	3.2
	Guadalupe	21.2	20.8	18.3	18.8
	Verde	6.9	4.1	2.8	3.9
		Standard Deviation of Seasonal Streamflow			
Standard deviation of seasonal streamflow	Haw	9.5	9.0	5.6	8.9
	Deep	23.5	21.3	14.7	17.3
	Guadalupe	45.4	50.3	40.4	55.0
	Verde	27.8	28.2	1.8	9.6
		Standard Deviation of 3 Day Peak Flow			
Standard deviation of 3-day peak flow	Haw	75.5	68.3	71.4	103.3
	Deep	142.6	138.1	138.1 157.5	157.3
	Guadalupe	216.8	267.1	240.5	260.9
	Verde	313.4	340.8	17.0	169.6
		Standard Deviation of 7 Day Low Flow			
Standard deviation of 7-low low flow	Haw	2.8	2.2	0.9	1.1
	Deep	7.4	5.6	1.3	2.0
	Guadalupe	10.1	9.1	9.2	8.2
	Verde	1.3	1.3	0.7	0.8

[a]Corresponding station names and numbers are in Table 1. (Unit: cubic meters per second)

Table 3. Seasonal Statistics of two Observed Hydrologic Variables of GW Depth for the Target Basins During the Control Period[a]

	DJF	MAN	JJA	SON
		Seasonal GW Depth		
Haw	13.22	17.61	5.82	13.03
Guadalupe	17.61	17.32	17.07	16.78
Verde	5.82	5.49	5.98	6.13
		Standard Deviation of Seasonal GW Depth		
Haw	0.60	0.71	0.69	0.61
Guadalupe	0.94	0.79	0.87	0.91
Verde	0.48	0.70	0.47	0.26

[a]Corresponding station names and numbers are in Table 1. (Unit: meters)

in streams subjected to minimal anthropogenic influences such as pumping and upstream storage [*Sankarasubramanian and Vogel*, 2002; *Vogel and Sankarasubramanian*, 2000]. Groundwater depth are procured from the USGS climate-groundwater response network, which comprises wells that are minimally influenced by pumping and storage. Station locations and periods of streamflow and groundwater data sets considered for this study are given in Table 1. Six seasonal statistics of the observed streamflow during the control period are shown in Table 2, and two seasonal statistics of the observed groundwater depth (GW depth) during the control period are shown in Table 3. Guadalupe River basin is the only watershed that has no significant seasonality on observed streamflow variables unlike the other basins that have clear seasonality. The changes in these eight hydrologic variables are projected to be decomposed by the different sources of errors in this study. The details on these eight variables are described in section 3.1.

2.3.2. GCM Precipitation and Temperature

Historic simulations of monthly precipitation and temperature series for 56 years (1950–2005) were obtained from a suite of 32 ensemble members from 11 GCM models of CMIP5 (shown in Table 4). Large spatial scale outputs from GCMs which were bias corrected to 1/8° by BCSD (monthly bias correction and spatial disaggregation) by Bureau of Reclamation (BOR) [*Reclamation*, 2014] were obtained for the four target basins. This ensured both observed and GCM climate projections having the same spatial resolution for forcings into PIHM.

2.3.3. GIS Data Sets

PIHM also requires GIS information regarding heterogeneity in hydrogeology, topography, and land use. Watershed boundary of eight-digit hydrologic unit code, terrain data on digital elevation, and land cover classification data were downloaded from the USGS national map viewer and download platform webpage (http://nationalmap.gov/viewer.html/). Soil classification data were obtained through the geospatial data gateway webpage of Natural Resources Conservation Service (NRCS) (http://datagateway.nrcs.usda.gov/). In absence of a more reliable data set, distributed hydrogeological properties were assumed to mirror spatial distribution of soil types. All spatially distributed data sets were converted into raster files for loading into the PIHMgis.

2.4. Calibration and Validation of PIHM

PIHM parameters were calibrated for the four target basins using observed precipitation and temperature time series at 1/8° for the control period (1956–1980). Manual calibration of hydrogeologic parameters such

Table 4. Details of the Selected 11 GCMs From the CMIP5 Historical Simulations [*Taylor et al.*, 2012a]

IPCC Model ID	Modeling Agency	# of Ensemble	Reference
CNRM_cm5	Centre National de Recherches Meteorologiques, France	1	*Voldoire et al.* [2013]
CSIRO_mk3_6	Commonwealth Scientific and Industrial Research Organization, Australia	10	*Jeffrey et al.* [2013]
GFDL_cm5	Geophysical Fluid Dynamics Laboratory, USA	5	*Yang et al.* [2013]
GFDL_esm2g	Geophysical Fluid Dynamics Laboratory, USA	1	*Yang et al.* [2013]
GISS_e2_r	NASA Goddard Institute for Space Studies, USA	1	*Chandler et al.* [2013]
IPSL_cm5a_lr	Institute Pierre-Simon Laplace, France	4	*Dufresne et al.* [2013]
MIROC_esm	Japan Agency for Marine-Earth Science and Technology, Atmosphere and Ocean Research Institute (The University of Tokyo), Japan	1	*Watanabe et al.* [2011]
MPI_esm_lr	Max Planck Institute for Meteorology, Germany	3	*Giorgetta et al.* [2013]
MRI_cgcm3	Meteorological Research Institute, Japan	1	*Yukimoto et al.* [2012]
NCAR_ccsm4	National Center for Atmospheric Research, USA	4	*Gent et al.* [2011]

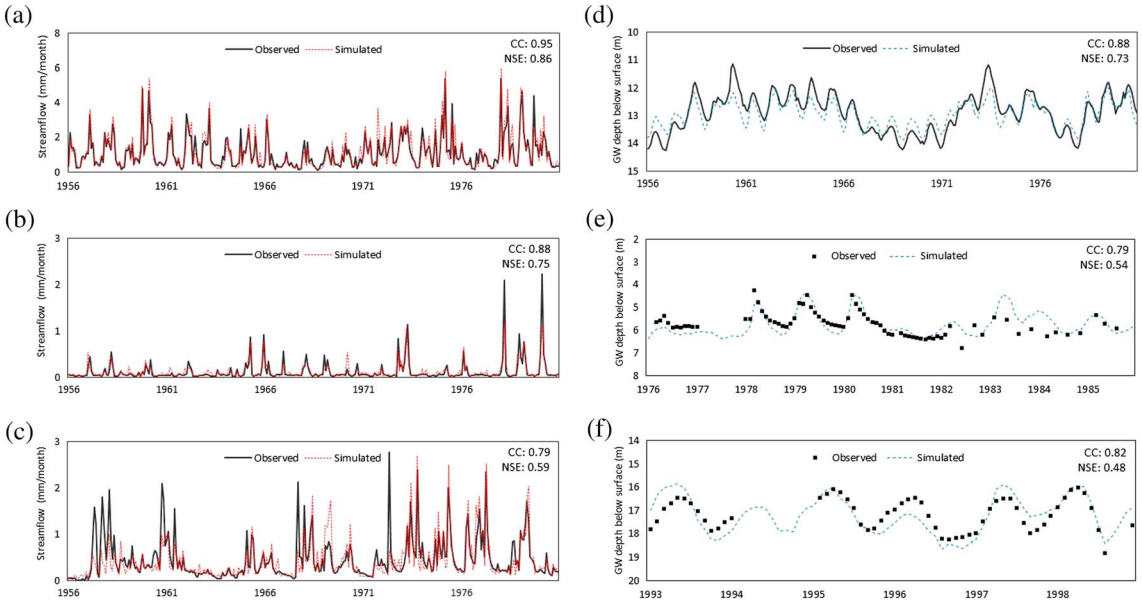

Figure 2. Performance of PIHM in simulating observed monthly (a–c) streamflow and (d–f) groundwater over the selected target basins (Haw River: (Figures 2a and 2d); Verde River: (Figures 2b and 2e); Guadalupe River: (Figures 2c and 2f)). Correlation coefficient (CC) and Nash-Sutcliffe efficiency (NSE) between the observed and the simulated time series are provided under each figure.

as soil hydraulic conductivity, macroporosity, and soil retention parameters was performed uniformly across the model domain to ensure modeled streamflow and groundwater variations were captured well. The simulated streamflow and groundwater were compared with the monthly observed streamflow and groundwater depth available at specific stations over the target basins. Figure 2 shows comparison of monthly time series of observed and PIHM simulated streamflow and groundwater depth. While the PIHM was able to capture the variability in GW depth extremely well (most relevant to this study), it had difficulty matching the observed mean values representing the equilibrium state of GW depth. Thus, constant bias corrections were applied to the simulated mean-monthly GW depth values. Delta values, i.e., mean GW depth correction factors, for Haw, Verde, and Guadalupe River were 12.24, 4.45, and 16.47 (m), respectively. Readers refer to Figure S2 in the supporting information for the bias correction of the groundwater depth in Haw River basin. For evaluating the model performance, correlation coefficient (CC) and Nash-Sutcliffe efficiency (NSE) values of monthly streamflow and GW depth were computed for each target basin (shown in Table 5). In spite of using manual calibration procedure, PIHM simulations of streamflow and GW depth were reasonably good in all the

Table 5. Evaluation of the Model Performance for Each Season: Correlation Coefficient and Nash-Sutcliffe Efficiency Values of Monthly Streamflow and GW Depth for Each Target Basin

		Calibration (1956–1980)								Validation (1981–2005)							
		CC				NSE				CC				NSE			
Watershed	Station Name/Number	DJF	MAM	JJA	SON	DJF	MAM	JJA	SON	DJF	MAM	JJA	SON	DJF	MAM	JJA	SON
Streamflow																	
Haw River	At Haw River	0.95	0.93	0.94	0.97	0.84	0.82	0.86	0.92	0.94	0.86	0.88	0.94	0.77	0.74	0.73	0.86
Deep River	At Moncure	0.94	0.96	0.97	0.96	0.83	0.87	0.93	0.90	0.93	0.97	0.93	0.96	0.53	0.84	0.76	0.83
Guadalupe River	At Victoria	0.91	0.69	0.80	0.76	0.81	0.45	0.60	0.51	0.82	0.70	0.69	0.82	0.65	0.42	0.47	0.65
Verde River	Above Horseshoe dam	0.89	0.79	0.89	0.89	0.74	0.61	0.73	0.78	0.80	0.92	0.90	0.92	0.53	0.65	0.80	0.85
Groundwater																	
Haw River	USGS 355522079043001	0.82	0.80	0.77	0.77	0.63	0.59	0.56	0.57	0.70	0.69	0.68	0.67	0.48	0.47	0.45	0.45
Guadalupe River[a]	TWDB 8017502	0.82				0.48											
Verde River[a]	USGS 341408111212901	0.79				0.54											

[a]Calibration periods of Guadalupe and Verde River groundwater depth are 1993–1998 and 1978–1985, respectively. And correlation coefficient (CC) and Nash-Sutcliffe efficiency (NSE) for each season are not shown due to lack of observed data period.

target basins. Overall, performance of streamflow simulations was better than that of GW depth (shown in Table 5). PIHM simulations in Haw and Deep River watersheds, located in humid climate, showed better performance than the other two basins.

3. Methodology

3.1. Experimental Design for Error Decomposition

Our primary focus is in quantifying various sources of errors arising from the model chain by comparing the observed changes in hydrologic variables with the estimated changes in hydrologic variables based on a retrospective analyses. For this purpose, we obtained projections of streamflow and groundwater from PIHM forced with CMIP5 BCSD projections disaggregated to daily series for the 55 year period (1951–2005). Excluding first 5 years simulation as a spin-up period, we considered 1956–1980 as the control period and 1981–2005 as the target period for estimating the changes in streamflow and groundwater depth. Future projections were not analyzed in this study since our interest is in decomposing the errors in estimating the changes in hydrologic attributes with the observed changes in hydrologic attributes between the control period and target period. PIHM parameters for all four target basins were calibrated with observed streamflow and groundwater depth for the control period (1956–1980) and then streamflow and groundwater depth were simulated for the target period (1981–2005). Target period is considered as the retrospective "projection" for quantifying the errors arising from the model chain. Hereafter, "projection" in this study represents PIHM estimates of streamflow and groundwater for the target period (1981–2005). Figure 3 illustrates an overall experimental design for out analyses on the different sources of errors that arise in projecting streamflow and groundwater depth using GCM forcing data. Three different model chains having different daily precipitation and temperature forcings were used to run the PIHM over the target period for quantifying the errors due to different modelling steps that matches the spatiotemporal resolution of the climate data to the required spatial (1/8°) and temporal (daily) scales for PIHM (Figure 3):

1. *Error due to hydrologic model (PIHM) (Model chain (a)):* Observed gridded daily precipitation and temperature series at 1/8° scale [*Maurer et al*., 2002] were forced with PIHM.
2. *Error due to disaggregation and hydrologic model (Model chain (b)):* Temporally disaggregated daily precipitation and temperature series from observed monthly data at 1/8° based on the approach by *Prairie et al*. [2007] were used as forcings. In order to estimate the errors in projection due to the temporal disaggregation scheme alone, daily observed precipitation and temperature series at 1/8° were first aggregated to monthly time step and then temporally disaggregated back to the daily time step. Thus, errors in the disaggregated observed time series primarily arise from the disaggregation scheme, and it gets transferred during the hydrologic simulation. Statistical disaggregation based on *k*-nearest neighbors (*k*-NN) algorithm [*Prairie et al*., 2007] was employed in this study. By considering observed monthly precipitation and temperature on the conditioning variable, *k* nearest neighbors were selected out of the entire historical time series based on the estimated distance between the conditioning variable and the historical time series over the entire period 1956 to 2005 in a leave-one-out cross validation. For instance, in order to select "*k*" nearest neighbors for January 1956, monthly precipitation for the remaining 49 years were considered—leaving out the conditioning point January 1956—for developing an ensemble. Then the daily series corresponding to the monthly series identified from *k* neighbors were resampled by assigning different weights based on Lall and Sharma kernel [*Lall and Sharma*, 1996]. For further details of the temporal disaggregation based on *k*-NN approach, see *Prairie et al*. [2007] and *Sinha and Sankarasubramanian* [2013].
3. *Error due to GCM downscaling, disaggregation, and hydrologic model (Model chain (c)):* Temporally disaggregated daily precipitation and temperature series from 32 ensemble members of monthly GCM series at 1/8° were used as forcings. It is noted that the GCM forcing data used in this study naturally contain the part of downscaling error in the model chain since the CMIP5 climate projections were downloaded to $1° \times 1°$, which are further interpolated to $1/8° \times 1/8°$ by BOR. *Reclamation* [2014] considered simple quantile mapping for downscaling large-scale climate variable to watershed scale. Readers are referred to *Reclamation* [2014] for more details about the spatially downscaled CMIP5 climate projections.

Other forcing series such as wind speed, relative humidity, vapor pressure, and solar radiation were kept same as daily mean series of model-simulated daily series driven by observed precipitation, and temperature across all three model configurations.

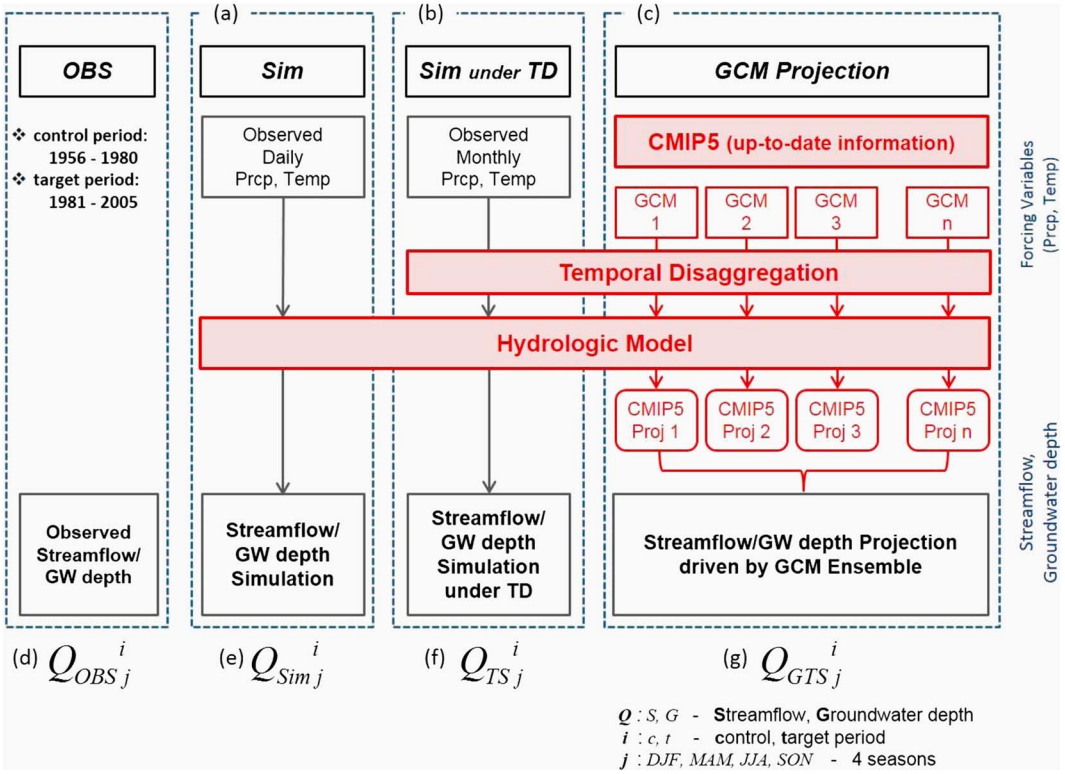

Figure 3. Experimental design for quantifying the sources of errors in developing seasonal streamflow and groundwater depth projections using near-term climate change information.

Each model chain projects eight hydrologic variables: (1) seasonal mean streamflow, (2) seasonal mean GW depth, (3) standard deviation of seasonal streamflow, (4) standard deviation of GW depth, (5) seasonal mean 3 day peak streamflow, (6) standard deviation of seasonal 3 day peak streamflow, (7) seasonal mean 7 day low streamflow, and (8) standard deviation of seasonal 7 day low streamflow. For obtaining the changes in the above eight attributes between the control period and the target period, we considered the changes in the respective statistics obtained from observed streamflow/GW depth as the baseline for comparison. Since observed GW depth is not available continuously for Verde and Guadalupe River basins, we considered simulated GW depth series from PIHM as the baseline. Hence, we obtained the changes in groundwater attributes from the simulated daily groundwater series for the two basins.

The eight hydrologic variables simulated by PIHM using observed daily forcings (Figure 3a) are denoted as $Q_{\mathrm{Sim}_j^i}$ (Figure 3e) where $i = c, t$ with "c" denoting the control period (1956–1980), and "t" denoting target period (1981–2005) and j = DJF (December, January, and February), MAM (March, April, and May), JJA (June, July, and August), and SON (September, October, and November)—representing four different seasons. From these simulated values, the bias in estimating these variables was calculated by comparing with the observed values. Next, the eight different hydrologic variables, $Q_{\mathrm{TS}_j^i}$, (Figure 3f) were obtained from streamflow and groundwater estimates from PIHM forced with daily disaggregated time series from observed monthly precipitation (Figure 3b). Thus, the difference between Figures 3e and 3f is considered as the error added due to temporal disaggregation scheme. Finally, we also estimated the projections of eight variables, $Q_{\mathrm{GTS}_j^i}$, (Figure 3g) were obtained from streamflow and groundwater estimates from PIHM forced with daily GCM forcings which were disaggregated from monthly GCM forcings from the BOR site (Figure 3c). The difference between Figure 3f and 3g provides the errors due to GCM forcings alone. Thus, the proposed experimental design helps us to quantify the errors arising from different steps in the model chain in translating the large-scale climate information to basin-scale changes in hydrologic variables.

3.2. Error Decomposition Metrics

3.2.1. Decomposition of Projection Errors

Following the decomposition procedures suggested by *Sinha et al*. [2014] and *Mazrooei et al*. [2015] for understanding the dominant sources of error in seasonal streamflow forecasts, the difference between observed and projected hydrologic variables could be linearly decomposed into three different sources of errors based on equation (1). Readers refer to Text S1 and Figure S1 in the supporting information for the validation of the linear decomposition.

$$Q_{\mathrm{OBS}_j}^{i} = Q_{\mathrm{GTS}_j}^{i} + \varepsilon_{\mathrm{GCM}_j}^{i} + \varepsilon_{\mathrm{TD}_j}^{i} + \varepsilon_{\mathrm{Sim}_j}^{i} \tag{1}$$

where $\varepsilon_{\mathrm{Sim}_j}^{i}$, $\varepsilon_{\mathrm{TD}_j}^{i}$, and $\varepsilon_{\mathrm{GCM}_j}^{i}$ are errors due to PIHM simulation, temporal disaggregation, and GCM forcings for *j* season in *i* period, respectively. Each of these errors on the selected hydrologic variables could be obtained sequentially as follows (equations (2)–(4)):

$$Q_{\mathrm{OBS}_j}^{i} = Q_{\mathrm{Sim}_j}^{i} + \varepsilon_{\mathrm{Sim}_j}^{i} \tag{2}$$

$$Q_{\mathrm{Sim}_j}^{i} = Q_{\mathrm{TS}_j}^{i} + \varepsilon_{\mathrm{TD}_j}^{i} \tag{3}$$

$$Q_{\mathrm{TD}_j}^{i} = Q_{\mathrm{GTS}_j}^{i} + \varepsilon_{\mathrm{GCM}_j}^{i} \tag{4}$$

In other words, Q_{GTS} is the streamflow/GW depth attributes having the error due to GCM forcings, temporal disaggregation, and hydrologic model all together. Q_{TS} is the streamflow/GW depth attributes having the error due to both temporal disaggregation and hydrologic model. Q_{Sim} is the streamflow/GW depth attributes having the error due to hydrologic model alone. With regard to error terms, $\varepsilon_{\mathrm{GCM}}$ is the error due to GCM forcings alone, $\varepsilon_{\mathrm{TD}}$ is the error due to temporal disaggregation alone, and $\varepsilon_{\mathrm{Sim}}$ is the error due to hydrologic model alone. Thus, the sum of these errors, $\varepsilon_{\mathrm{GCM}} + \varepsilon_{\mathrm{TD}} + \varepsilon_{\mathrm{Sim}}$, is the total error from the model chain in projecting changes in hydrologic variables using GCM forcings.

3.2.2. Decomposition of Errors in Projecting the Changes in Hydrologic Variables

As discussed earlier, studies have addressed uncertainty embedded on GCM-driven hydroclimate projections arising from the model chain based on ANOVA techniques. Our study, however, is aimed at analyzing how different sources of errors from the model chain propagate by comparing the observed hydrologic variables with the projected estimates. Given that all model estimates have inherent bias in estimating the observed values, climate change studies typically focus on the projected changes in hydrologic variables, which could provide the potential change from the observed period [*Harding et al*., 2012; *Aich et al*., 2013; *Ficklin et al*., 2013; *Yang et al*., 2014]. Hence, we addressed how the errors from the model chain propagate in estimating the change in projections of the considered eight hydrologic variables. Thus, we also quantified how three different sources of errors—GCM forcings, temporal disaggregation, and PIHM simulation—propagate along the model chain and affect the projected changes in hydrologic variables. Observed changes of the hydrologic variables, $\delta_{\mathrm{OBS}j}$, for season *j* between the target and the control period can be written as

$$\delta_{\mathrm{OBS}j} = Q_{\mathrm{OBS}_j}^{\mathrm{target}} - Q_{\mathrm{OBS}_j}^{\mathrm{control}} \tag{5}$$

Similarly, changes in the hydrologic variables estimated by the hydrologic model using (1) observed forcings ($\delta_{\mathrm{Sim}j}$), (2) temporally disaggregated observed forcings ($\delta_{\mathrm{TD}j}$), and (3) temporally disaggregated GCM forcings ($\delta_{\mathrm{GCM}j}$) are calculated by substituting equation (1) into equation (5), we get

$$\delta_{OBSj} = \left(Q_{GTS_j}^{\mathrm{target}} + \varepsilon_{\mathrm{GCM}_j}^{\mathrm{target}} + \varepsilon_{\mathrm{GCM}_j}^{\mathrm{target}} + \varepsilon_{\mathrm{GCM}_j}^{\mathrm{target}}\right) - \left(Q_{\mathrm{GTS}_j}^{\mathrm{control}} + \varepsilon_{\mathrm{GCM}_j}^{\mathrm{control}} + \varepsilon_{\mathrm{GCM}_j}^{\mathrm{control}} + \varepsilon_{\mathrm{GCM}_j}^{\mathrm{control}}\right) \tag{6}$$

$$\delta_{\mathrm{OBS}j} = \delta_{\mathrm{GTS}j} + \delta_{\varepsilon_{\mathrm{GCM}}} + \delta_{\varepsilon_{\mathrm{TD}}} + \delta_{\varepsilon_{\mathrm{Sim}}} \tag{7}$$

where $\delta_{\mathrm{GTS}} = Q_{\mathrm{GTS}_j}^{\mathrm{target}} - Q_{\mathrm{GTS}_j}^{\mathrm{control}}$, $\delta_{\varepsilon_{\mathrm{GCM}}} = \varepsilon_{\mathrm{GCM}_j}^{\mathrm{target}} - \varepsilon_{\mathrm{GCM}_j}^{\mathrm{control}}$, $\delta_{\varepsilon_{\mathrm{TD}}} = \varepsilon_{\mathrm{TD}_j}^{\mathrm{target}} - \varepsilon_{\mathrm{TD}_j}^{\mathrm{control}}$, and $\delta_{\varepsilon_{\mathrm{Sim}}} = \varepsilon_{\mathrm{Sim}_j}^{\mathrm{target}} - \varepsilon_{\mathrm{Sim}_j}^{\mathrm{control}}$.

Thus, the change in the observation ($\delta_{\mathrm{OBS}j}$) between the two periods can be explained by the change in GCM projections ($\delta_{\mathrm{GTS}j}$) and the sum of the changes in errors that arise in the model chain ($\delta_{\varepsilon_{\mathrm{GCM}}} + \delta_{\varepsilon_{\mathrm{TD}}} + \delta_{\varepsilon_{\mathrm{Sim}}}$). Hereinafter, we define the change in error (CIE) as the difference in the error (δ_{ε}) due to a particular modeling step between the control period and the target period. Thus, using the metrics defined in section 3.2, we decomposed both the errors as well as how the errors change between the two time periods in translating large-scale information to local scale.

4. Results and Analysis

Daily streamflow and GW depth series for the control and target periods were obtained by using three different forcings (as discussed in section 3) for all the four target basins. In total, eight seasonal hydrologic attributes were derived from the estimated daily streamflow and GW depth series under three different model chains, $Q_{\mathrm{Sim}_j}^{i}$, $Q_{\mathrm{TS}_j}^{i}$, and $Q_{\mathrm{GTS}_j}^{i}$, for each target basin. Since climate change studies typically focus on the estimation of changes in hydrologic variables (δ), we first present projection errors with the decomposition metrics defined in section 3.2.1. Following that, we discuss how errors in the estimation under target and control periods are decomposed based on the metrics defined in section 3.2.2.

4.1. Errors in the Estimation of Changes in Hydrologic Variables

Figure 4 shows how the ensemble of GCM projections ($\delta_{\mathrm{GTS}j}$) captures the observed changes in each seasonal streamflow attribute. With respect to mean seasonal streamflow (Figure 4a), GCM projections were not able to capture the observed changes. Especially, in the case of Haw River basin, GCM projections cannot even get the direction of the observed change correctly for any season. It is also important to note that projection range—distance between first and third quartile values—of the ensemble members in small watersheds, Haw and Deep River basins, are much wider compared to Guadalupe and Verde River basins, which are relatively large watersheds. This indicates that projection driven by GCM forcings may induce larger uncertainty, particularly in smaller watersheds. This is consistent with other studies focusing on climate change impacts [*Christensen et al*., 2007; *Foley*, 2010; *Corney et al*., 2013]. Of all the basins, the projected and observed changes in mean seasonal flow agree reasonably well for the Verde River basin even though the observed change is very small in the basin. Similarly, the observed and projected changes in mean seasonal flow are in line during all the seasons except summer. Further, ensemble mean of projected changes underestimated the observed change in all the seasons except fall (i.e., ensemble mean of the projected changes did not imply significant changes in projection regardless of its predictability). On estimating the seasonal streamflow variability (Figure 4b), projections show similar pattern as that of seasonal mean projection. In general, information from GCM projections underestimates the observed variability of seasonal streamflow. For Verde River basin, since there is no noticeable change in the observed streamflow series as well as in the GCM streamflow projections, it is hard to evaluate the performance of the GCM projections on both mean seasonal streamflow and variability in seasonal streamflow.

Even though we calibrated and validated model using historic observed data set, there were some differences in PIHM performance between the control and the target period. If there are large differences in hydrologic model performances between the control and target (future) period, we can say current climate regime is not same to the future period (from hydrologic model performance points of view). By comparing the seasonal NSE values between control and target periods in Table 4 along with Figure 5, we found that estimation of changes in variables are affected by the changes in hydrologic model performance between control and target period at some extent. In other words, when there was larger difference between NSE values of control and target period (regardless of the values of NSE for each control or target period), the model performance for estimation of changes in variables was poorer at some extent. For instance, NSE values of spring/summer season in control and target period for Guadalupe basin were 0.45/0.60 and 0.42/0.47, respectively. Thus, the changes in NSE values are −0.03/−0.13. Even though model performance was quite poor in spring season for both period, changes in NSE value was low and the model performance for estimation of changes in mean streamflow and variability in spring season was very good (Figures 4a and 4b). On the contrary, the performance in summer season was poor given that the changes in NSE values was much larger than spring season. Even though we used historic data sets for near-term climate change, the changes in climate regime would be intensified in the future as discussed in *Wasko and Sharma* [2015] when it comes to long-term future. In this regard, model configuration for the future period would be one of the challenges in climate change studies up to the end of 21st century.

With respect to capturing the changes in the statistics of hydrologic extremes such as 3 day peak and 7 day low seasonal streamflow (Figures 4c to 4f), information from GCM were not able to project the observed change. Comparing Figures 4a and 4b with 4c–4f in Figure 4, we infer the bias in estimating the observed change in hydrologic extremes being much larger than the bias in estimating the observed mean seasonal and interannual variability in streamflow. Ensemble mean values of GCM projections of hydrologic extremes were generally close to the horizontal axes which implies no change. Thus, no significant change was estimated even though observed changes being exhibited in the mean and standard deviation of 3 day peak flows. We also considered how the climate information captures the observed change in low-flow characteristics.

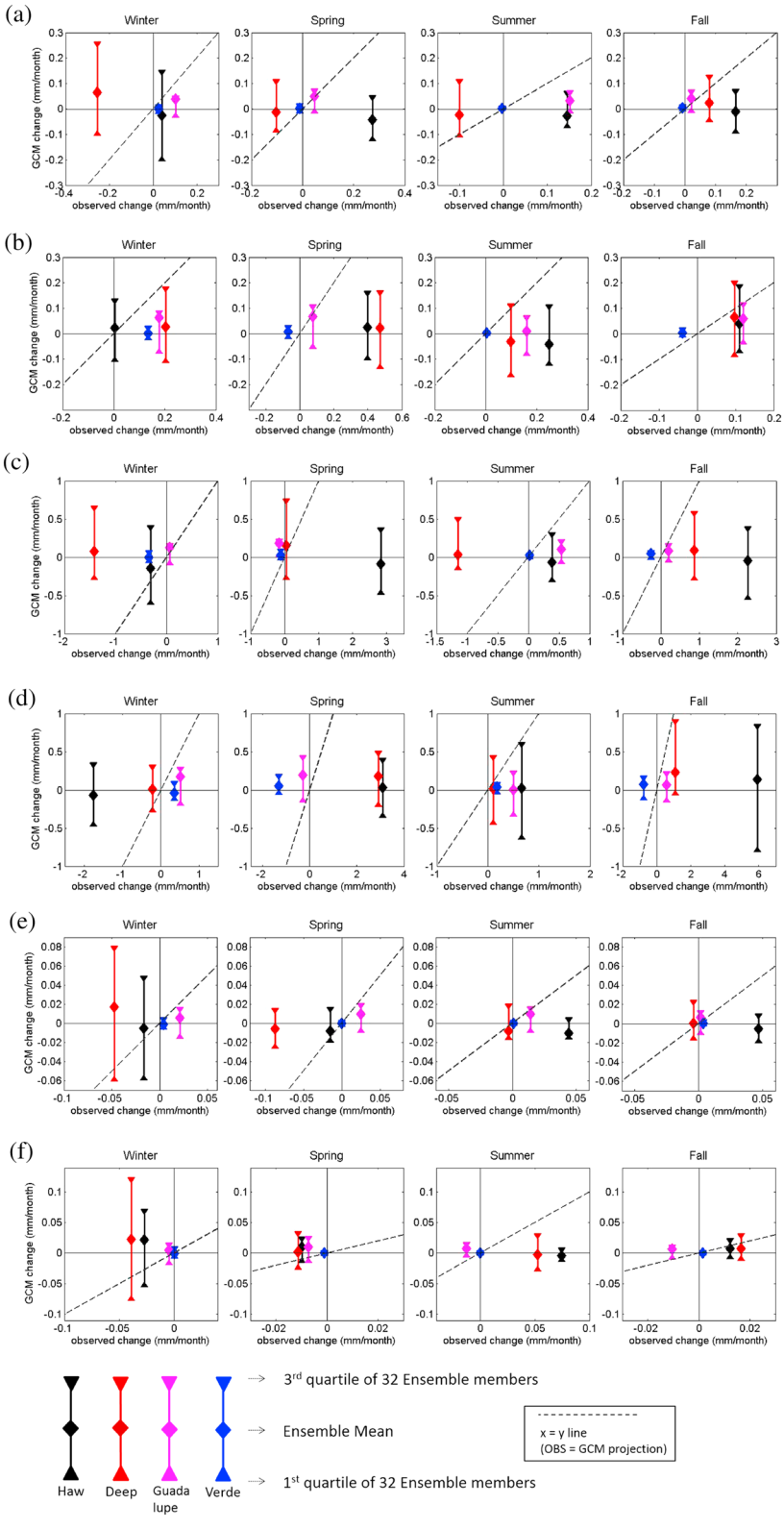

Figure 4. Comparison between observed change (*x* axes) and the estimated changes (*y* axes, δ_{GTS_j}) from PIHM forced with 32-ensemble BCSD GCM projections (changes between 1956–1980 and 1981–2005): (a) mean and (b) standard deviation of seasonal streamflow, (c) mean and (d) standard deviation of 3 day maximum seasonal streamflow, and (e) mean and (f) standard deviation of 7 day minimum flows over the four seasons. Dotted line represents the observed change being equal to the estimated change.

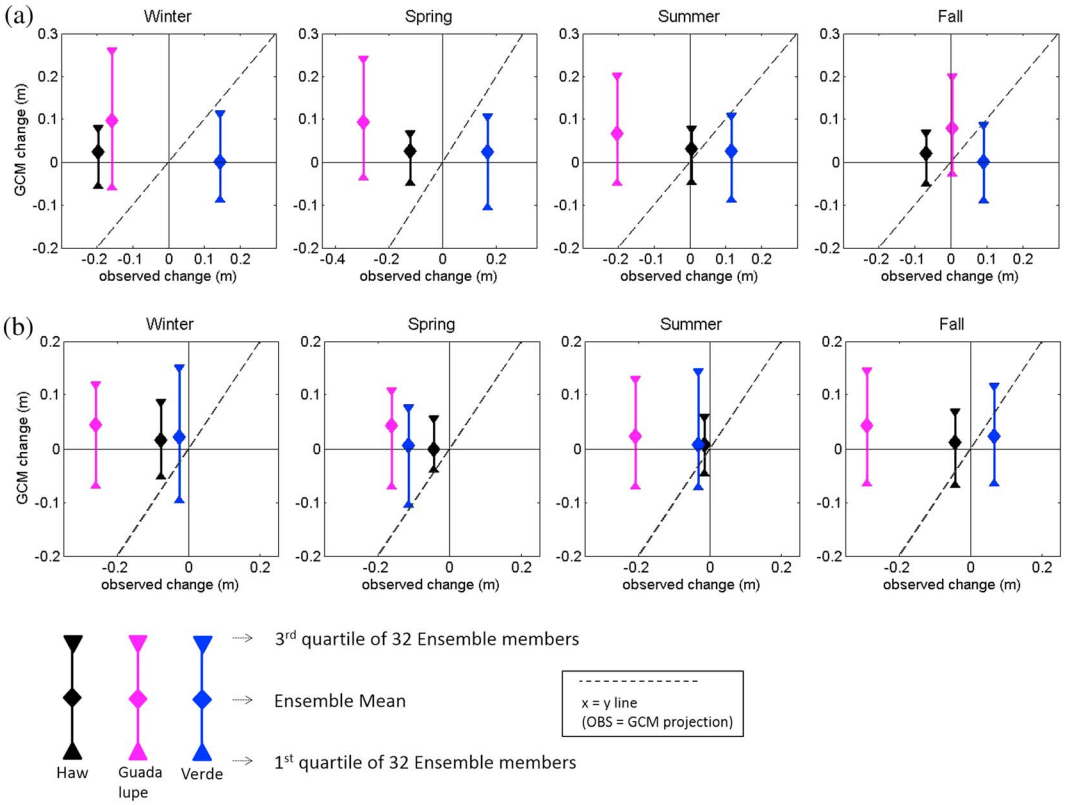

Figure 5. Comparison between observed change (*x* axes) and the estimated change (*y* axes, δ_{GTSj}) from PIHM forced with 32-ensemble BCSD GCM projections (changes between 1956–1980 and 1981–2005): (a) mean and (b) standard deviation of seasonal GW depth over the four seasons.

For this purpose, we compared the mean and standard deviation of 7 day low flows projected by the GCMs with the observed statistics of 7 day low flows for each season. Given the observed mean and standard deviation of 7 day low flows were small, the projected range from 32 member ensemble was also very small. Comparing the ability to project across different seasons, the projected 7- day low-flow statistics correspond slightly better during the spring and summer seasons.

Similar to streamflow projections, the changes in GW depth projected by GCM were not able to capture the observed changes (shown in Figure 5). Mean seasonal GW depth (Figure 5a) of Verde River basin increased by around 0.1 m for all the seasons, but GCM projections do not show any change. Moreover, the mean seasonal GW depth projections for Haw and Guadalupe River basin were not even able to get the direction of the observed change correctly. The projected mean GW depth showed an increase, while the observed mean GW depth showed a decrease. Further, GCM projections also were not able to predict the direction of the observed change of GW depth variability (Figure 5b). Fall season in Verde River is the only season that GCM projections capture the direction in the observed change of GW depth variability correctly.

It is important that the projected changes in hydrologic variables provide the ability of GCM projections (δ_{GTSj} in equation (7)) in explaining the observed change considering all the errors introduced through the model chain. Our analysis shows that GCM projections show large errors in capturing the change in small humid basins, Haw and Deep, from the Sunbelt east. Since these two watersheds are relatively smaller, the ensemble spreads of Haw and Deep River basins were generally wider than the other two basins. For the semiarid Guadalupe River basin, GCM projections relatively capture both the direction and magnitude of the observed changes in mean seasonal streamflow and the variability of seasonal streamflow. However, the GCM projections of GW depth for Guadalupe River were not as good as streamflow projections. The Verde River basin, an arid basin from the Sunbelt west, exhibits the smallest ensemble spread in the projected change for almost all variables. This could be partly due to larger catchment area and also due to arid hydroclimatic conditions, which critically depends on temperature (as opposed to precipitation) in estimating streamflow, leading

to reduced uncertainty in projections. Studies have shown that temperature predicted by GCMs has less uncertainty compared to the precipitation [e.g., *Devineni and Sankarasubramanian*, 2010; *Goddard et al.*, 2013; *Gonçalves et al.*, 2014]. Hence, projected changes in various hydrologic attributes exhibit smaller ensemble spread for the Verde River basin compared to other basins.

4.2. Decomposition of Sources of Errors in Projecting the Changes in Hydrologic Variables

The unexplained change by GCM projections is equal to the sum of the changes in three different sources of error (equation (7)). Thus, GCM's inability in estimating the observed change can be explained by the sum of the CIE from different sources in the model chain between control and target periods. Error decomposition results of seasonal streamflow change projections are presented in Figure 6. The solid line in each plot denotes the value of unexplained change by GCM projections ($\delta_{\mathrm{OBS}j} - \delta_{\mathrm{GTS}j}$). Each bar chart represents the change value in errors from different sources (e.g., $\delta_{\varepsilon_{\mathrm{Sim}}} = \varepsilon_{\mathrm{Sim}_j}^{\mathrm{target}} - \varepsilon_{\mathrm{Sim}_j}^{\mathrm{control}}$). For mean seasonal streamflow and variability of seasonal streamflow (Figures 6a and 6b), the primary source of error arises from the changes in error due to GCM forcing, hereinafter CIE-GCM ($\delta_{\varepsilon_{\mathrm{GCM}}}$) for three seasons—winter, spring, and summer—over Haw, Guadalupe, and Verde River basins. In these three basins, the changes in error due to hydrologic model (PIHM) simulation, hereinafter CIE-SIM ($\delta_{\varepsilon_{\mathrm{Sim}}}$) dominates during the fall season. In the case of Deep River basin, CIE-GCM ($\delta_{\varepsilon_{\mathrm{GCM}}}$) is high during the spring season, but the CIE-SIM ($\delta_{\varepsilon_{\mathrm{Sim}}}$) dominates during the rest of the season. Overall, the changes in error due to temporal disaggregation, hereinafter CIE-TD ($\delta_{\varepsilon_{\mathrm{TD}}}$) are smaller than the other sources except in winter for Guadalupe River basin. This is to be expected as the mean and variance of seasonal streamflow primarily depend on the mean and variance of seasonal forcings as opposed to their interseasonal variability, which usually associates with the disaggregation error. Thus, the observed change in mean seasonal streamflow and variability in seasonal streamflow (Figures 6a and 6b) primarily arise from the CIE-GCM ($\delta_{\varepsilon_{\mathrm{GCM}}}$) which includes both the error from the climate change projections as well as from the spatial downscaling scheme in the model chain since we use the downscaled climate information for forcing the PIHM. Following that, the next source of error arise from the inability of the hydrologic model to capture the observed change in mean and variance of seasonal streamflow.

On the other hand, decomposing the errors in projecting the changes in hydrologic extremes (shown in Figures 6c–6f), we infer that the CIE-SIM ($\delta_{\varepsilon_{\mathrm{Sim}}}$), followed by CIE-TD ($\delta_{\varepsilon_{\mathrm{TD}}}$), account for the most unexplained change in hydrologic extremes in almost all the four seasons over all the basins except the Guadalupe River basin. This does not imply that the errors arising from the GCM projections are relatively small. It only implies that the CIE-GCM ($\delta_{\varepsilon_{\mathrm{GCM}}}$) between the two periods is relatively small in explaining the change in hydrologic extremes. One possible reason for the dominant source being hydrologic model is because the calibration of PIHM parameters primarily focused on evaluating the skill in predicting monthly streamflow and groundwater. Changes in *R* bias (shown in equation (8) for season *j*) of all the six seasonal streamflow variables are presented in Table 6. The values of the changes in *R* bias represent the ability of PIHM in estimating the changes in the hydrologic variables. For instance, lower value of changes in *R* bias represents that model skill is quite constant between the control and target periods, which means that the model is reliable to estimate the changes between the two periods. We found that the values of hydrologic extremes are mostly larger than the values of seasonal mean flow in terms of the changes in *R* bias. Thus, it infers that changes in errors arising from PIHM are relatively large in explaining the changes in hydrologic extremes. Further, it is logical to expect that the disaggregation being a significant source in predicting the extremes since disaggregation scheme develops the required daily forcings, which primarily account for the skill in predicting extremes. In the case of Guadalupe River basin, the CIE-GCM ($\delta_{\varepsilon_{\mathrm{GCM}}}$) dominates across the most seasons. Following that, we also infer that CIE-TD ($\delta_{\varepsilon_{\mathrm{TD}}}$) being the significant source in accounting for the unexplained changes in predicting the extremes. The primary reason behind this is that the ability of PIHM in predicting the observed hydrologic extremes being much better compared to other basins. As shown in Table 6, the values of changes in *R* bias of Guadalupe River basin are mostly smaller than the other three basins over all the seasons. Hence, the CIE-GCM ($\delta_{\varepsilon_{\mathrm{GCM}}}$) account for the most unexplained change in projecting the hydrologic extremes (Figures 6c–6f).

$$\delta_{\text{R-bias}j} = \left\{ \left(Q_{\mathrm{Sim}_j}^{\mathrm{target}} - Q_{\mathrm{OBS}_j}^{\mathrm{target}} \right) / Q_{\mathrm{OBS}_j}^{\mathrm{target}} \right\} - \left\{ \left(Q_{\mathrm{Sim}_j}^{\mathrm{control}} - Q_{\mathrm{OBS}_j}^{\mathrm{control}} \right) / Q_{\mathrm{OBS}_j}^{\mathrm{control}} \right\} \tag{8}$$

Decomposing the errors in projecting the changes in mean and variability of seasonal GW depth (Figure 7) clearly show that CIE-GCM ($\delta_{\varepsilon_{\mathrm{GCM}}}$) account for the most unexplained observed changes in groundwater attributes over all the seasons and all the basins except for the Verde River basin. This is similar to the

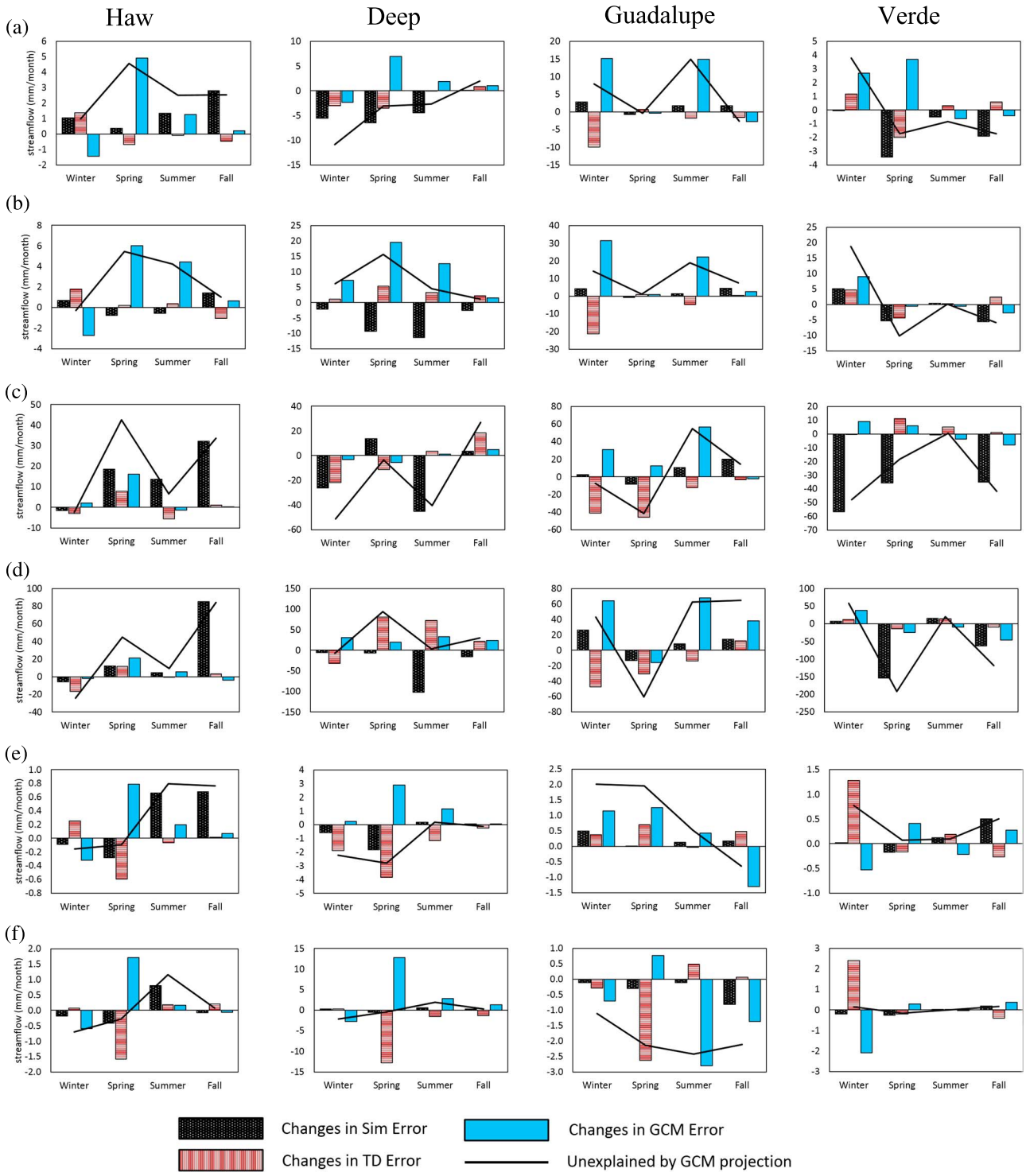

Figure 6. Decomposition of different sources of errors in projecting (a) mean and (b) standard deviation of seasonal streamflow, (c) mean and (d) standard deviation of 3 day peak seasonal streamflow, and (e) mean and (f) standard deviation of 7 day low flows over the four seasons using near-term climate change information.

streamflow indicating that CIE-GCM ($\delta_{\varepsilon_{GCM}}$) play a critical role for explaining the observed change in mean seasonal attributes. Since there is no significant seasonality on streamflow and GW depth in the Guadalupe River basin, a similar pattern of CIE from different sources is exhibited across all the seasons. In the case of Verde River basin, both CIE-GCM ($\delta_{\varepsilon_{GCM}}$) and CIE-TD ($\delta_{\varepsilon_{TD}}$) account for the unexplained change in seasonal

Table 6. Changes in *R* Bias of the Six Seasonal Streamflow Variables Between the Control and the Target Periods[a]

	DJF	MAN	JJA	SON
		Seasonal Mean Streamflow		
Haw	−0.045	−0.021	−0.117	−0.218
Deep	0.102	0.115	0.219	−0.008
Guadalupe	−0.007	0.012	0.001	−0.015
Verde	0.004	0.140	0.099	0.210
		Seasonal Mean 3 Day Peak Flow		
Haw	0.010	−0.154	−0.186	−0.233
Deep	0.064	−0.040	0.219	0.012
Guadalupe	−0.003	0.026	−0.015	−0.040
Verde	0.197	0.242	−0.010	0.654
		Seasonal Mean 7 Day Low Flow		
Haw	0.007	0.052	−0.294	−0.286
Deep	0.040	0.186	−0.029	0.001
Guadalupe	0.004	0.006	0.002	−0.006
Verde	0.008	0.043	−0.030	−0.074
		Standard Deviation of Seasonal Streamflow		
Haw	−0.073	−0.027	0.002	−0.136
Deep	0.019	0.143	0.603	0.104
Guadalupe	−0.002	0.014	0.013	0.002
Verde	0.031	0.131	−0.107	0.965
		Standard Deviation of 3 Day Peak Flow		
Haw	0.025	−0.103	−0.050	−0.310
Deep	0.044	−0.079	0.641	0.119
Guadalupe	−0.055	0.050	−0.010	0.031
Verde	0.060	0.398	−0.257	0.418
		Standard Deviation of 7 Day Low Flow		
Haw	0.021	0.157	−0.376	0.097
Deep	−0.083	0.068	−0.555	−0.212
Guadalupe	0.002	0.028	−0.002	0.064
Verde	0.068	0.252	0.022	−0.045

[a]Corresponding station names and numbers are in Table 1.

groundwater attributes. This is partly due to the significant seasonality in both streamflow and groundwater exhibited at the Verde River basin. Deep River basin is not shown since observed time series of GW depth was not available for the basin.

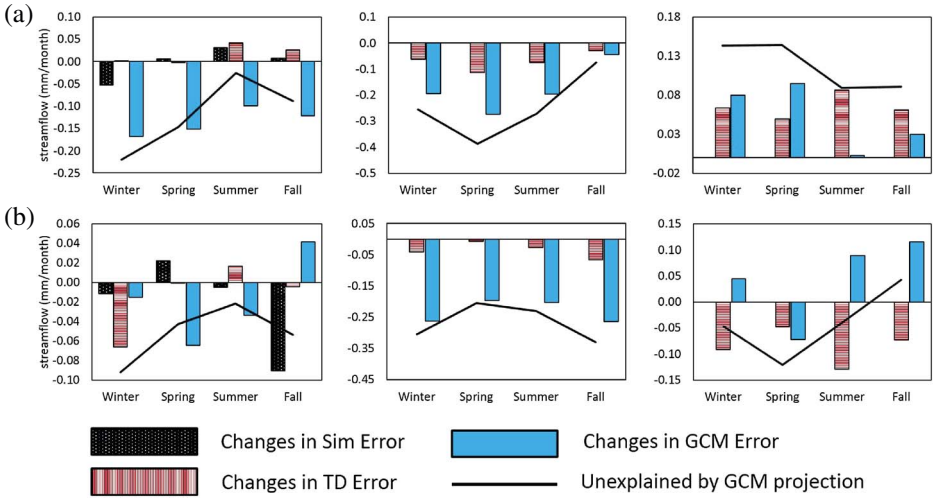

Figure 7. Decomposition of different sources of errors in projecting (a) mean and (b) standard deviation of seasonal groundwater depth over the four seasons using near-term climate change information.

To summarize the findings on decomposing various sources of errors that impact the estimation of changes in hydrologic attributes, we infer the following: (1) CIE-GCM ($\delta_{\varepsilon_{GCM}}$) is the main source of error accounting for the unexplained changes in mean and variability of seasonal hydrologic attributes, since climate forcings being the primary information to explain the changes; (2) CIE-SIM ($\delta_{\varepsilon_{Sim}}$) and CIE-TD ($\delta_{\varepsilon_{TD}}$) play an important role in predicting the changes in hydrologic extremes, since daily forcings are critical for predicting extremes; and (3) the sources of error also vary significantly depending on the seasonality and the hydroclimatic regime (i.e., arid/humid) of the basin.

4.3. Discussion—Dominant Sources of Errors in Projecting the Changes in Hydrologic Variables

The main motivation of this study is to develop a framework for decomposing the various sources of errors arising from the model chain in projecting the changes in hydrologic attributes using climate change information. Given climate change impacts are typically estimated by downscaling large-scale information to local scale through a series of model chain, we proposed metrics that systematically decomposes different sources of errors in projecting the changes in seasonal hydrologic attributes arising from the model chain. The proposed metrics basically assume that the errors from different steps in the model chain are independent and could be systematically decomposed to obtain the errors due to different sources (equations (1)-(4)). Given our interest under near-term climate change is in projecting the changes in hydrologic attributes, we used the decomposed errors (in equation (1)) to estimate the changes in error characteristics from different sources (equations (5)–(7)) by comparing with the observed changes in the respective attributes. This provides us the basic framework and a general set of equations for understanding the magnitude and direction of errors arising from the model chain. In this analysis, we considered the error due to GCM and downscaling into one single source, but one could estimate the downscaling error alone, following the approach of *Sinha et al*. [2014] and *Mazrooei et al*. [2015], by upscaling the observed precipitation and temperature to the spatial resolution of BCSD (i.e., $1° \times 1°$) and then applying the downscaling procedure, quantile mapping, adapted by BOR. We did not estimate the downscaling error separately here, since we expect it to be very small as found by *Sinha et al*. [2014] and *Mazrooei et al*. [2015]. Though we applied the proposed equations (1)–(7) for four test basins, in principle it can be applied to quantify the errors in estimating the observed flows and in estimating the changes in hydrologic attributes for any given watershed. Further, one could also apply these equations for any type of model chain including dynamic downscaling.

To understand the dominant source of error over the four selected basins, we plot the fractions of each sources of errors for seasonal streamflow attributes (Figure 8) and for seasonal hydrologic extremes of streamflow (Figure 9). Figures 8 and 9 obtain the fraction (f_ψ) due to a particular source, ψ (i.e., GCM or TD or SIM), using the following expression:

$$f_\psi = \frac{\left|\delta_{\varepsilon_\psi}\right|}{\left|\delta_{\varepsilon_{GCM}}\right| + \left|\delta_{\varepsilon_{TD}}\right| + \left|\delta_{\varepsilon_{Sim}}\right|} \tag{9}$$

The main idea of this analysis is to look at the magnitude of CIE from a particular source in relation to the combined CIE from all the sources and also compare their relative magnitudes across the basins. Deep river is not plotted in Figures 8 and 9 due to similarity of results with Haw River. From Figure 8, CIE-GCM ($\delta_{\varepsilon_{GCM}}$) (blue color) dominate in the most basins except during the fall season, which is the low-flow season in most basins. Specifically, Haw River basin, located under humid hydroclimatic regime, shows greater portion of CIE-GCM ($\delta_{\varepsilon_{GCM}}$)—i.e., larger fraction of blue color—in comparison to Verde River basin, which is located in arid hydroclimatic regime, in all the seasons except fall during which CIE-SIM ($\delta_{\varepsilon_{Sim}}$) dominates. In general, contribution of CIE-GCM ($\delta_{\varepsilon_{GCM}}$) tends to decrease under low-flow season (i.e., fall season) and arid hydroclimatic regime. This is partly due to the reason that humid (arid) basins rely more on precipitation (temperature), which is poorly (relatively well) estimated by both historical and hindcasts of GCM [*Goddard et al*., 2013; *Gonçalves et al*., 2014].

With regard to estimating the changes in hydrologic extremes, contributions of CIE-SIM ($\delta_{\varepsilon_{Sim}}$) and CIE-TD ($\delta_{\varepsilon_{TD}}$) were increased especially for 3 day peak flow as shown in Figure 9 (increased fractions of dotted gray and lined red pies that represent CIE-SIM ($\delta_{\varepsilon_{Sim}}$) and CIE-TD ($\delta_{\varepsilon_{TD}}$), respectively). Given that PIHM is driven by daily forcings, estimation of changes in hydrologic extremes is much more affected by the skill of temporal disaggregation and hydrologic model performance on daily series simulation. For instance, disaggregated climate forcings from monthly to daily are unable to capture the relevant peaks in precipitation resulting in increased

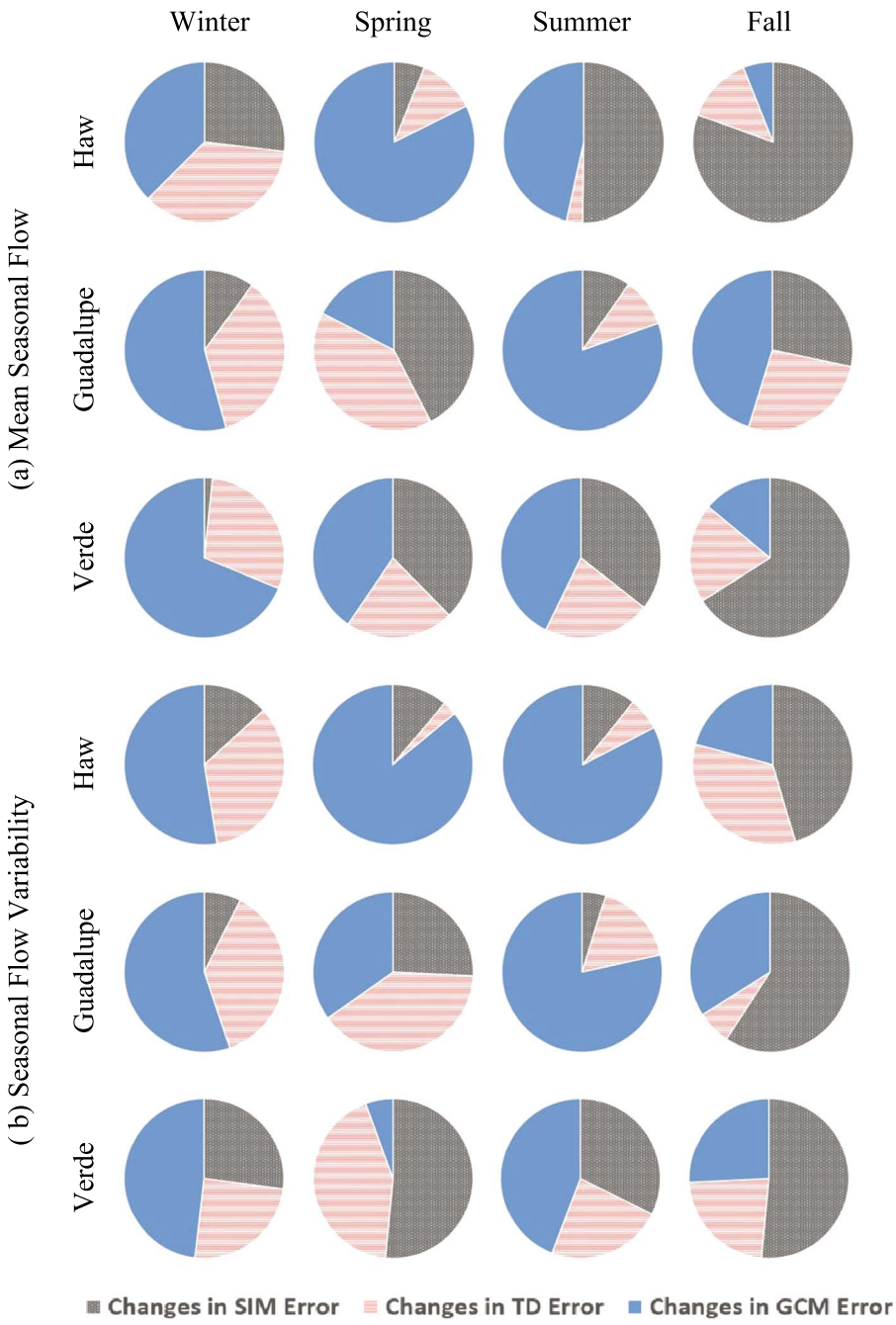

Figure 8. Fraction of three different sources of errors in projecting changes in (a) mean and (b) standard deviation of seasonal streamflow over the four seasons using near-term climate change information: Haw, Guadalupe, and Verde River basins.

CIE-TD ($\delta_{\varepsilon_{TD}}$) in capturing the changes in the hydrologic extremes. Further, the reason for the increased CIE-SIM ($\delta_{\varepsilon_{Sim}}$) is partly due to the reason that most hydrologic models are calibrated for monthly performance not based on their ability to simulate the hydrologic extremes. In the context of seasonal projections, changes in errors arising from hydrologic model simulation and temporal disaggregation scheme are typically cancelled out upon aggregation of daily series to seasonal time scale. Thus, in the context of predicting changes in hydrologic extremes, particularly peak flow characteristics, it may be desirable to consider alternate approaches such as stochastic models that directly relate the climate information with the observed seasonal peaks [*Sankarasubramanian and Lall*, 2003].

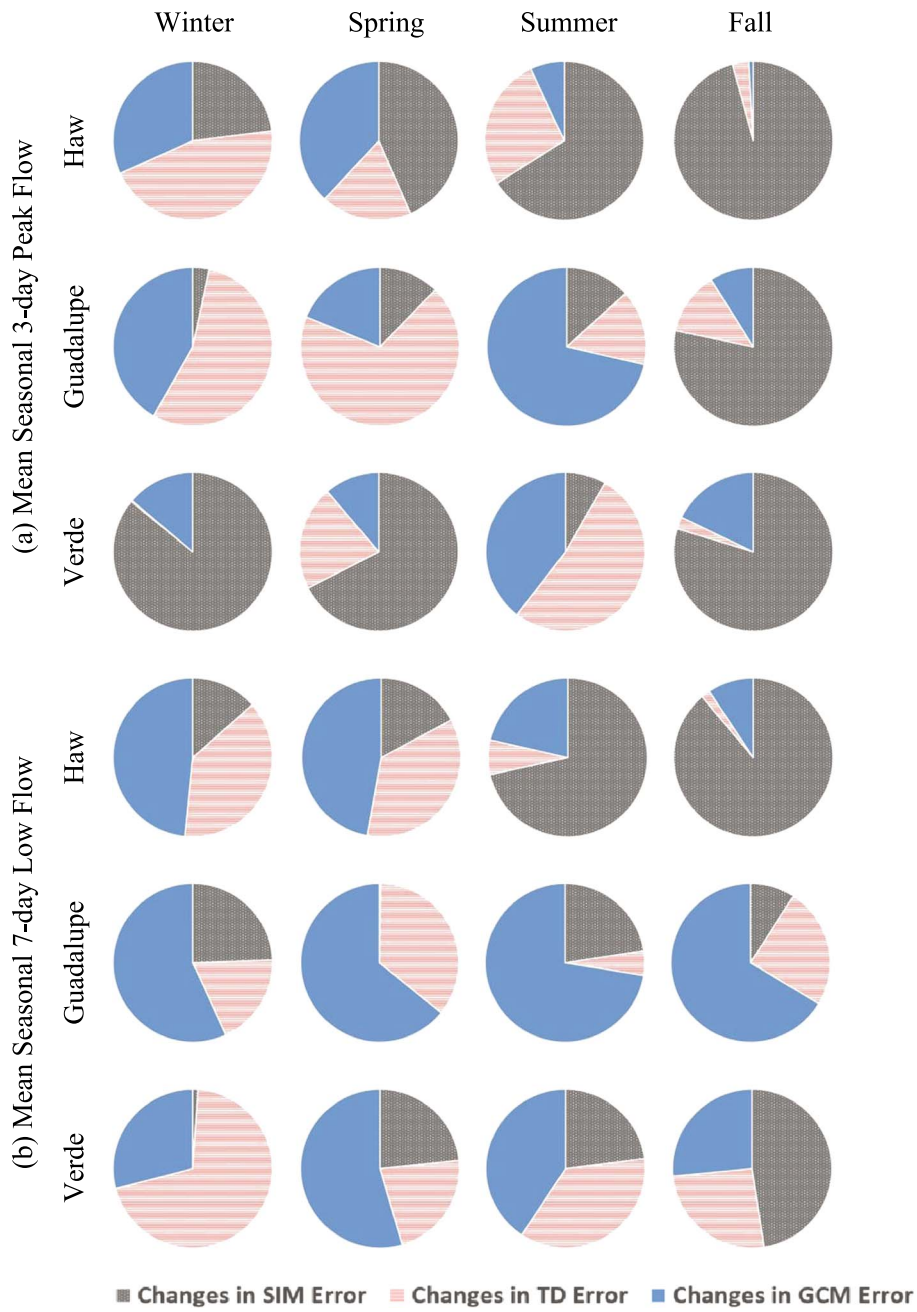

Figure 9. Fraction of three different sources of errors in projecting changes in mean seasonal (a) 3 day peak and (b) 7 day low streamflow over the four seasons using near-term climate change information: Haw, Guadalupe, and Verde River basins.

In addition, a particular modeling (e.g., temporal disaggregation and GCM data sets) in the chain can be alternated by state-of-the-art schemes, while we applied *k*-NN resampling for temporal disaggregation and BCSD for GCM date sets that have been widely used. For example, *Johnson and Sharma* [2012] proposed nesting bias correction (NBC) method that corrects means, standard deviations, and lag-1 autocorrelations so that it was able to improve representation of distributional and persistence attributes. While *Johnson and Sharma* [2015] found that the both bias correction methods, NBC and quantile mapping which is a basis of BCSD, reduced the prediction errors in GCM simulations, they discussed that quantile mapping method can result in distortion of persistence attributes such as drought. Thus, NBC approach should be considered for an appropriate bias correction method for climate change impact studies. In this study, however, we retained GCM data

sets which were bias corrected based on quantile mapping since we used only historic simulation data sets of GCMs under consideration of near-term climate change.

Given that we are considering near-term climate change under an assumption that there is no significant changes in climate regime, we did not consider climate nonstationarity. Thus, we assumed calibrated parameters using control period are valid for the target period. For reference, if there is drastic difference in climatic conditions in the future, choice of calibration length should be carefully considered [*Vaze et al.*, 2010]. Plus, if this study is extended to the long-term climate change such as up to the end of 21st century, temporal disaggregation scheme used in this study would have a critical limitation that cannot sample potential extremes which are beyond the observations. Thus, as *Wasko et al.* [2015] discussed, potential extremes in the future should be deliberately considered for the long-term climate change studies. Besides, *Sharma and Mehrotra* [2014] introduced partial information-partial weighting (PI-PW) framework as an alternative formulating prediction models for natural system so that overcome current limitations of *k*-NN algorithm. Readers refer to *Sharma and Mehrotra* [2014] for details on the PI-PW framework.

5. Conclusions

This study proposed a systematic decomposition procedure for quantifying the errors arising from various sources in the model chain in projecting the changes in hydrologic attributes using near-term climate change projections. The motivation is to understand errors from different sources so that a particular modeling (e.g., temporal disaggregation) in the chain could be improved. The findings from the application of the decomposition procedure over four target basins could be summarized as follows: (1) changes in the observed hydrologic attributes were not captured well by the change in GCM projections, (2) projected changes in hydrologic variables forced by a set of multiple GCMs generally underestimate observed changes of hydrologic attributes, (3) changes in error due to GCM forcing (temporal disaggregation scheme and hydrologic model simulation) play an important role in capturing the changes in mean and variability of seasonal streamflow (hydrologic extremes of streamflow), (4) comparing across the watersheds, the smaller watersheds lead to larger GCM ensemble spreads indicating higher uncertainty in projecting the changes in hydrologic attributes, and (5) semiarid/arid (humid) basins show reduced (enlarged) uncertainty with narrower (wider) ensemble spread in projecting the changes in hydrologic attributes as arid (humid) basins rely more on temperature (precipitation), which is better (poorly) simulated by GCMs.

Acknowledgments

We first would like to thank anonymous reviewers for their valuable comments on the manuscript. This research is supported in part by the National Science Foundation under grant 1204368. Any opinions, findings, and conclusions or recommendations expressed in this material are those of the authors and do not necessarily reflect the views of the National Science Foundation. Gridded observed precipitation and temperature data are available at Ed Maurer's webpage (http://www.engr.scu.edu/~emaurer/gridded_obs/index_gridded_obs.html) Historic simulations of monthly precipitation and temperature series are downloadable from CMIP5 webpage (http://gdo-dcp.ucllnl.org/downscaled_cmip_projections). Streamflow and GW depth data for the target basins are available at USGS Water Data webpage (http://waterdata.usgs.gov/nwis), while groundwater data for Guadalupe River basin are downloadable from Water Data for Texas webpage (http://www.waterdatafortexas.org/groundwater) For GIS data set, watershed boundary shape files, and terrain data on digital elevation, land cover classification data are available at the USGS national map viewer and download platform (http://nationalmap.gov/viewer.html) Along with land cover data, soil classification data are available at the geospatial data gateway webpage of NRCS (http://datagateway.nrcs.usda.gov).

References

Aich, V., et al. (2013), Comparing impacts of climate change on streamflow in four large African river basins, *Hydrol. Earth Syst. Sci. Discuss.*, *10*(11), 13,005–13,052.

Bhatt, G., M. Kumar, and C. J. Duffy (2014), A tightly coupled GIS and distributed hydrologic modeling framework, *Environ. Modell. Software*, *62*, 70–84.

Bosshard, T., M. Carambia, K. Goergen, S. Kotlarski, P. Krahe, M. Zappa, and C. Schär (2013), Quantifying uncertainty sources in an ensemble of hydrological climate-impact projections, *Water Resour. Res.*, *49*, 1523–1536, doi:10.1029/2011WR011533.

Chandler, M. A., L. E. Sohl, J. A. Jonas, H. J. Dowsett, and M. Kelley (2013), Simulations of the mid-Pliocene Warm Period using two versions of the NASA/GISS ModelE2-R Coupled Model, *Geosci. Model Dev.*, *6*(2), 517–531.

Chen, X., M. Kumar, and B. McGlynn (2015), Variations in streamflow response to large hurricane-season storms in a southeastern US watershed, *J. Hydrometeorol.*, *16*, 55–69.

Cheng, C. S., Q. Li, G. Li, and H. Auld (2012), Possible impacts of climate change on daily streamflow and extremes at local scale in Ontario, Canada. Part II: Future projection, *Atmos. Clim. Sci.*, *2*(04), 427.

Cherkauer, K. A., and T. Sinha (2010), Hydrologic impacts of projected future climate change in the Lake Michigan Region, *J. Great Lakes Res.*, *36*(2), 33–50.

Christensen, J. H., T. R. Carter, M. Rummukainen, and G. Amanatidis (2007), Evaluating the performance and utility of regional climate models: The PRUDENCE project, *Clim. Change*, *81*(1), 1–6.

Christensen, N. S., A. W. Wood, N. Voison, D. P. Lettenmaier, and R. N. Palmer (2004), The effect of climate change on the hydrology and water resources of the Colorado river basin, *Clim. Change*, *62*, 337–363.

Clark, A. K., C. D. Blome, and R. R. Morris (2014), Geology and hydrostratigraphy of Guadalupe River State Park and Honey Creek State Natural Area, Kendall and Comal Counties, Texas, U.S. Geol. Surv. Sci. Invest. Map, 3303, 8 p.

Corney, S., M. Grose, J. C. Bennett, C. White, J. Katzfey, J. McGregor, G. Holz, and N. L. Bindoff (2013), Performance of downscaled regional climate simulations using a variable-resolution regional climate model: Tasmania as a test case, *J. Geophys. Res. Atmos.*, *118*, 11,936–11,950, doi:10.1002/2013JD020087.

Devineni, N., and A. Sankarasubramanian (2010), Improving the prediction of winter precipitation and temperature over the continental United States: Role of ENSO state in developing multimodel combinations, *Mon. Weather Rev.*, *138*(6), 2447–2468.

Dufresne, J. L., et al. (2013), Climate change projections using the IPSL-CM5 Earth System Model: From CMIP3 to CMIP5, *Clim. Dyn.*, *40*(9–10), 2123–2165.

Ficklin, D. L., I. T. Stewart, and E. P. Maurer (2013), Climate Change Impacts on Streamflow and Subbasin-Scale Hydrology in the Upper Colorado River Basin, *PLoS One*, *8*(8), e71297, doi:10.1371/journal.pone.0071297.
Foley, A. M. (2010), Uncertainty in regional climate modelling: A review, *Prog. Phys. Geogr.*, *37*(2), 178–205.
Fowler, H. J., C. G. Kilsby, and J. Stunell (2007), Modeling the impacts of projected future climate change on water resources in north-west England, *Hydrol. Earth Syst. Sci.*, *11*, 1115–1126.
Gent, P. R., et al. (2011), The community climate system model version 4, *J. Clim.*, *24*(19), 4973–4991.
Giorgetta, M. A., et al. (2013), Climate and carbon cycle changes from 1850 to 2100 in MPI-ESM simulations for the Coupled Model Intercomparison Project phase 5, *J. Adv. Model. Earth Syst.*, *5*(3), 572–597.
Goddard, L., et al. (2013), A verification framework for interannual-to-decadal predictions experiments, *Clim. Dyn.*, *40*(1–2), 245–272.
Gonçalves, M., A. Barrera-Escoda, D. Guerreiro, J. M. Baldasano, and J. Cunillera (2014), Seasonal to yearly assessment of temperature and precipitation trends in the North Western Mediterranean Basin by dynamical downscaling of climate scenarios at high resolution (1971–2050), *Clim. Change*, *122*(1–2), 243–256.
Harding, B. L., A. W. Wood, and J. R. Prairie (2012), The implications of climate change scenario selection for future streamflow projection in the Upper Colorado River Basin, *Hydrol. Earth Syst. Sci.*, *16*(11), 3989–4007.
Hawkins, E., and R. Sutton (2009), The potential to narrow uncertainty in regional climate predictions, *Bull. Am. Meteorol. Soc.*, *90*(8), 1095–1107.
Jeffrey, S., L. Rotstayn, M. Collier, S. Dravitzki, C. Hamalainen, C. Moeseneder, K. K. Wong, and J. Syktus (2013), Australia's CMIP5 submission using the CSIRO-Mk3. 6 model, *Aust. Meteorol. Oceanogr. J.*, *63*, 1–13.
Johnson, F., and A. Sharma (2012), A nesting model for bias correction of variability at multiple time scales in general circulation model precipitation simulations, *Water Resour. Res.*, *48*, W01504, doi:10.1029/2011WR010464.
Johnson, F., and A. Sharma (2015), What are the impacts of bias correction on future drought projections?, *J. Hydrol.*, *525*, 472–485, doi:10.1016/j.jhydrol.2015.04.002.
Katz, R. W., P. F. Craigmile, P. Guttorp, M. Haran, B. Sansó, and M. L. Stein (2013), Uncertainty analysis in climate change assessments, *Nat. Clim. Change*, *3*(9), 769–771.
Kim, N. W., I. M. Chung, Y. S. Won, and J. G. Arnold (2008), Development and application of the integrated SWAT–MODFLOW model, *J. Hydrol.*, *356*(1–2), 1–16.
Kløve, B., et al. (2014), Climate change impacts on groundwater and dependent ecosystems, *J. Hydrol.*, *518*, 250–266.
Koutroulis, A. G., I. K. Tsanis, I. N. Daliakopoulos, and D. Jacob (2013), Impact of climate change on water resources status: A case study for Crete Island, Greece, *J. Hydrol.*, *479*, 146–158.
Kumar, M. (2009), Toward a hydrologic modeling system, PhD thesis, Pennsylvania State Univ. [Available at https://etda.libraries.psu.edu/paper/9870/.]
Lall, U., and A. Sharma (1996), A nearest neighbor bootstrap for resampling hydrologic time series, *Water Resour. Res.*, *32*(3), 679–693, doi:10.1029/95WR02966.
Li, W., A. Sankarasubramanian, R. S. Ranjithan, and E. D. Brill (2014), Improved regional water management utilizing climate forecasts: An interbasin transfer model with a risk management framework, *Water Resour. Res.*, *50*, 6810–6827, doi:10.1002/2013WR015248.
Maurer, E. P., and P. B. Duffy (2005), Uncertainty in projections of streamflow changes due to climate change in California, *Geophys. Res. Lett.*, *32*, L03704, doi:10.1029/2004GL021462.
Maurer, E. P., A. W. Wood, J. C. Adam, D. P. Lettenmaier, and B. Nijssen (2002), A long-term hydrologically based dataset of land surface fluxes and states for the conterminous Unites States, *J. Clim.*, *15*(22), 3237–3251.
Mazrooei, A., T. Sinha, A. Sankarasubramanian, S. Kumar, and C. D. Perters-Lidard (2015), Decomposition of sources of errors in seasonal streamflow forecasting over the US Sunbelt, *J. Geophys. Res. Atmos.*, *120*, 11,809–11,825, doi:10.1002/2015JD023687.
Minville, M., F. Brissette, and R. Leconte (2010), Impacts and uncertainty of climate change on water resource management of the Peribonka River System (Canada), *J. Water Res. Plann. Manage.*, *136*(3), 376–385.
Najafi, M. R., H. Moradkhani, and I. W. Jung (2011), Assessing the uncertainties of hydrologic model selection in climate change impact studies, *Hydrol. Processes*, *25*(18), 2814–2826.
Prairie, J., B. Rajagopalan, U. Lall, and T. Fulp (2007), A stochastic nonparametric technique for space-time disaggregation of streamflows, *Water Resour. Res.*, *43*, W03432, doi:10.1029/2005WR004721.
Qu, Y., and C. J. Duffy (2007), A semidiscrete finite volume formulation for multiprocess watershed simulation, *Water Resour. Res.*, *43*, W08419, doi:10.1029/2006WR005752.
Reclamation (2014), 'Downscaled CMIP3 and CMIP5 climate and hydrology projections: Release of hydrology projections, comparison with preceding information, and summary of user needs', prepared by the U.S. Dep. of the Interior, Bureau of Reclamation, Technical Services Center, Denver, Colo., 110 pp.
Sankarasubramanian, A., and R. M. Vogel (2002), Annual hydroclimatology of the United States, *Water Resour. Res.*, *38*(6), 1083, doi:10.1029/2001WR000619.
Sankarasubramanian, A., and U. Lall (2003), Flood Quantiles and Changing Climate: Seasonal forecasts and causal relations, *Water Resour. Res.*, *39*(5), 1134, doi:10.1029/2002WR001593.
Sharma, A., and R. Mehrotra (2014), An information theoretic alternative to model a natural system using observational information alone, *Water Resour. Res.*, *50*, 650–660, doi:10.1002/2013WR013845.
Shi, Y., K. J. Davis, C. J. Duffy, and X. Yu (2013), Development of a coupled land surface hydrologic model and evaluation at a critical zone observatory, *J. Hydrometeorol.*, *14*, 1401–1420.
Singh, H., T. Sinha, and A. Sankarasubramanian (2015), Impacts of near-term climate change and population growth on within-year reservoir systems, *J. Water Res. Plann. Manage.*, *141*(6), 04014078, doi:10.1061/(ASCE)WR.1943-5452.0000474.
Sinha, T., and A. Sankarasubramanian (2013), Role of climate forecasts and initial conditions in developing streamflow and soil moisture forecasts in a rainfall–runoff regime, *Hydrol. Earth Syst. Sci.*, *17*(2), 721–733.
Sinha, T., A. Sankarasubramanian, and A. Mazoorei (2014), Decomposition of sources of errors in monthly to seasonal streamflow forecasts in a rainfall-runoff regime, *J. Hydrometeorol.*, *15*, 2470–2483.
Taylor, K. E., R. J. Stouffer, and G. A. Meehl (2012a), An overview of CMIP5 and the experiment design, *Bull. Am. Meteorol. Soc.*, *93*(4), 485–498.
Taylor, R. G., et al. (2012b), Ground water and climate change, *Nat. Clim. Change*, *3*(4), 322–329.
Thompson, J. R., A. J. Green, D. G. Kingston, and S. N. Gosling (2013), Assessment of uncertainty in river flow projections for the Mekong River using multiple GCMs and hydrological models, *J. Hydrol.*, *486*, 1–30.
Vano, J. A., N. Voisin, L. Cuo, A. F. Hamlet, M. M. Elsner, R. N. Palmer, A. Polebitski, and D. P. Lettenmaier (2010), Climate change impacts on water management in the Puget Sound region, Washington State, USA, *Clim. Change*, *102*(1–2), 261–286.

Vaze, J., D. A. Post, F. H. S. Chiew, J. M. Perraud, N. R. Viney, and J. Teng (2010), Climate non-stationarity—Validity of calibrated rainfall-runoff models for use in climate change studies, *J. Hydrol.*, *394*(3–4), 447–457, doi:10.1016/j.jhydrol.2010.09.018.

Vicuna, S., E. P. Maurer, B. Joyce, J. A. Dracup, and D. Purkey (2007), The sensitivity of California water resources to climate change scenarios, *J. Am. Water Resour. Astron.*, *43*, 482–498.

Vogel, R. M., and A. Sankarasubramanian (2000), Spatial scaling properties of annual streamflow in the United States, *Hydrol. Sci. J.*, *45*(3), 465–476.

Voldoire, A., et al. (2013), The CNRM-CM5. 1 global climate model: Description and basic evaluation, *Clim. Dyn.*, *40*(9–10), 2091–2121.

Wang, R., M. Kumar, and D. Marks (2013), Anomalous trend in soil evaporation in a semi-arid, snow-dominated watershed, *Adv. Water Resour.*, *57*, 32–40.

Wasko, C., and A. Sharma (2015), Steeper temporal distribution of rain intensity at higher temperatures within Australian storms, *Nat. Geosci.*, *8*, 527–529, doi:10.1038/NGEO2456.

Wasko, C., A. Sharma, and F. Johnson (2015), Does storm duration modulate the extreme precipitation-temperature scaling relationship?, *Geophys. Res. Lett.*, *42*, 8783–8790, doi:10.1002/2015GL066274.

Watanabe, S., et al. (2011), MIROC-ESM 2010: Model description and basic results of CMIP5-20c3m experiments, *Geosci. Model Dev.*, *4*, 845–872.

Wilby, R. L., and I. Harris (2006), A framework for assessing uncertainties in climate change impacts: Low-flow scenarios for the River Thames, UK, *Water Resour. Res.*, *42*, W02419, doi:10.1029/2005WR004065.

Woldemeskel, F. M., A. Sharma, B. Sivakumar, and R. Mehrotra (2012), An error estimation method for precipitation and temperature projections for future climates, *J. Geophys. Res.*, *117*, D22104, doi:10.1029/2012JD018062.

Woldemeskel, F. M., A. Sharma, B. Sivakumar, and R. Mehrotra (2014), A framework to quantify GCM uncertainties for use in impact assessment studies, *J. Hydrol.*, *519*, 1453–1465, doi:10.1016/j.jhydrol.2014.09.025.

Yang, T., X. Wang, Z. Yu, V. Krysanova, X. Chen, F. W. Schwartz, and E. A. Sudicky (2014), Climate change and probabilistic scenario of streamflow extremes in an alpine region, *J. Geophys. Res. Atmos.*, *119*, 8535–8551, doi:10.1002/2014JD021824.

Yang, X., et al. (2013), A predictable AMO-like pattern in the GFDL fully coupled ensemble initialization and decadal forecasting system, *J. Clim.*, *26*(2), 650–661.

Yip, S., C. A. Ferro, D. B. Stephenson, and E. Hawkins (2011), A simple, coherent framework for partitioning uncertainty in climate predictions, *J. Clim.*, *24*(17), 4634–4643.

Yu, X., A. Lamacová, C. Duffy, P. Krám, J. Hruška, T. White, and G. Bhatt (2014), Modeling long term water yield effects of forest management in a Norway spruce forest, *Hydrol. Sci. J.*, *60*(2), 174–191.

Yukimoto, S., et al. (2012), A new global climate model of the Meteorological Research Institute: MRI-CGCM3—Model description and basic performance, *J. Meteorol. Soc. Jpn.*, *90A*, 23–64.

Zhu, T., and C. Ringler (2012), Climate change impacts on water availability and use in the Limpopo River Basin, *Water*, *4*, 63–84.